UC Berkeley
UC Berkeley Previously Published Works

Title
Understanding the Microscopic Structure of Counterion Condensation Near a Charged Polypeptoid Surface

Permalink
https://escholarship.org/uc/item/41f0j4sq

Journal
The Journal of Physical Chemistry Letters, 17(40)

ISSN
1948-7185

Authors
Zhang, Xiaohui
Liu, Luofu
Jiang, Xi
et al.

Publication Date
2026-10-08

DOI
10.1021/acs.jpclett.6c02156

Copyright Information
This work is made available under the terms of a Creative Commons Attribution License, available at https://creativecommons.org/licenses/by/4.0/

Peer reviewed

eScholarship.org Powered by the California Digital Library
University of California

Understanding the Microscopic Structure of Counterion Condensation Near a Charged Polypeptoid Surface

Xiaohui Zhang,[†,‡] Luofu Liu,[†] Xi Jiang,[‡] Ronald N. Zuckermann,[¶] David Prendergast,[¶] Nitash P. Balsara,[†,‡] and Rui Wang[*,†,‡]

†*Department of Chemical and Biomolecular Engineering, University of California, Berkeley, California 94720, United States*

‡*Materials Sciences Division, Lawrence Berkeley National Laboratory, Berkeley, California 94720, United States*

¶*Molecular Foundry, Lawrence Berkeley National Laboratory, Berkeley, California 94720, United States*

E-mail: ruiwang325@berkeley.edu

Abstract

The molecular-level study of the electrical double layer is key to understanding ion solvation, adsorption, and transport in many electrochemical and biological systems. Here, we combine the modified Gaussian renormalized fluctuation theory and molecular dynamics simulations to investigate the microscopic structure of counterion condensation near a charged nanofiber created by self-assembly of amphiphilic polypeptoids in water. Our theory shows a peak shift of the counterion distribution, indicating the existence of a water monolayer between condensed counterions and surface charges. Without any fitting parameters, the peak position and the shape of the counterion distribution predicted by our theory are in quantitative agreement with recent

experimental results using cryogenic electron microscopy. We provide a possible explanation for the underlying mechanism for the formation of such solvent-separated ion pairs as the image charge repulsion at an interface with a dielectric mismatch. This important feature arising from electrostatic fluctuations cannot be captured by either classical Poisson–Boltzmann theory or simulations using non-polarizable force fields.

The study of the electrical double layer (EDL) lies at the heart of colloidal and interfacial science, which affects a wealth of structural and dynamic properties in many physicochemical and biophysical systems.[1–5] The distribution and condensation of ions in the EDL are usually modeled by the classical Gouy–Chapman theory based on the Poisson–Boltzmann (PB) equation.[6,7] The classical theory is built upon the primitive model with ions immersed in a dielectric medium, describing the EDL at a continuum level.

There has been growing interest in the microscopic study of the double layer structure. The molecular details of the interplay between surface charges, salt ions, and water molecules are essential for ion solvation, adsorption, and transport. These play a vital role in understanding and fine-tuning electrocatalytic activity,[8] charge storage in supercapacitors,[9,10] and ion selectivity in biological channels.[11,12] Various experimental techniques, such as *in situ* nuclear magnetic resonance (NMR),[9,10] atomic force microscopy (AFM),[13,14] ambient-pressure X-ray photoelectron spectroscopy (APXPS),[15,16] neutron reflectometry (NR),[17] and scanning electrochemical potential microscopy (SECPM)[18] have been utilized to probe different charged surfaces and test the validity of the classical theory. Recently, Seidler *et al.*[19] used cryogenic electron microscopy (cryo-EM) to obtain atomic-scale images of condensed counterions near positively charged 9N-Nte$_6$-NBipe$_6$·Cl polypeptoid nanofibers. This polypeptoid consists of six hydrophilic Nte monomers (N-2-(2-(2-methoxyethoxy)ethoxy)ethylglycine), five hydrophobic NBipe monomers (N-(2-(4-biphenyl)ethyl)glycine), and an N-(2-(4-aminophenyl)ethyl)glycine monomer introduced at the ninth position from the N-terminus. The amine is protonated with hydrochloric acid to form the chloride salt. The chemical structure of the polypeptoid is shown in Figure 1(a). The polypeptoid self-assembles into crystalline nanofibers in water, where the strands adopt an extended

conformation and pack into rows. Two of these rows pack next to one another to form a bilayer nanofiber, where the charged aromatic groups are exposed to solvent. The authors found that the distribution of halogen counterions peaked at distances of about 5 Å away from the fixed positive charge (see the cryo-EM image in Figure 1(b)), indicating the presence of a layer of water molecules between surface charges and condensed ions. However, this experimental finding contradicts the prediction from the classical theory, where it is generally accepted that condensed counterions form close contact ion pairs as this would directly neutralize surface charges. The discrepancy suggests that the microscopic picture of the EDL, particularly the solvation structure of condensed counterions, remains unclear. The charged-interface/aqueous-solution system hence behaves in a more complicated way than the simple sum of its parts, highlighting the inadequacy of the classical PB theory in describing the EDL.[4]

Due to its mean-field nature, an obvious factor missing in the classical PB theory is the fluctuations of the electrostatic field. These fluctuations lead to the self energy of ions, which contains a local contribution in terms of the Born solvation energy and other long-range contributions.[20] In particular, near a surface with a dielectric mismatch, the distortion of the electrostatic potential at the interface, usually known as the "image charge effect", is an important component of the long-range part of the self energy. This is commonplace because of the much lower dielectric constant of polymers, lipid membranes, and colloidal particles ($\varepsilon \sim 1$) than that of the aqueous solution ($\varepsilon \sim 80$). Using weak-coupling theory, Wang and Wang predicted that image charge repulsion causes a depletion of counterions from the surface.[21,22] It should be noted that the image charge effect cannot be captured by either the classical PB theory or molecular simulations with non-polarizable force fields.[21,23,24] It is thus desirable to systematically incorporate this molecular-level image charge effect into the continuum classical theory to validate (or negate) experimental findings.

In this Letter, we address the puzzle of the microstructure of condensed counterions near a charged polypeptoid surface observed by Seidler *et al.*[19] Using the modified Gaussian renormalized fluctuation theory,[25,26] we show that the peak of the distribution of halogen counterions is shifted away from the charged surface toward the aqueous solution. Combining the theory with molecular

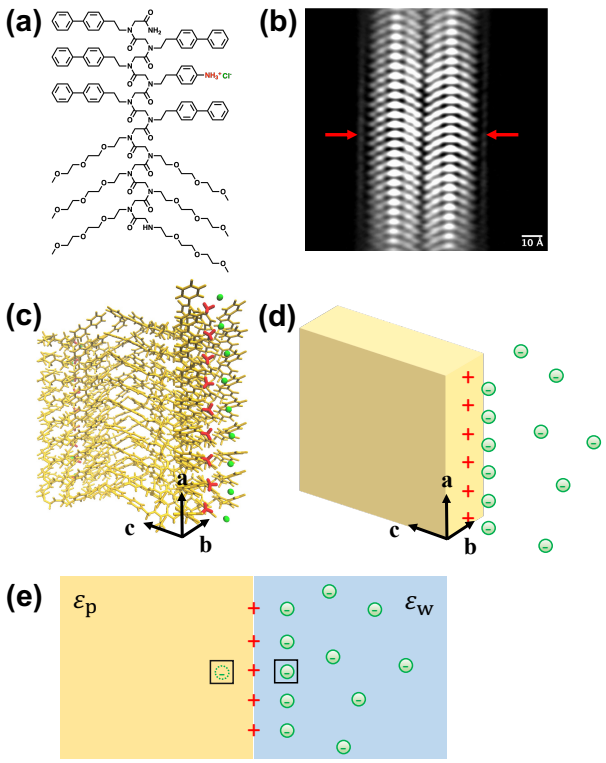


Figure 1: Schematic illustration of counterion condensation near a positively charged polypeptoid surface. (a) The chemical structure of 9N-Nte$_6$-NBipe$_6$·Cl polypeptoid. (b) Cryo-EM images of the nanofibers. The bright dotted lines show the presence of condensed Cl^- counterions, which are highlighted by the arrows. (c) Atomic model of crystalline polypeptoids with V-shaped motifs assembled in the a–c plane. Charged $-NH_3^+$ groups (red) are in the a–b plane and halogen counterions nearby are shown by green spheres. (d) A simplified model of a rectangular cuboid with uniform surface charges in the a–b plane. (e) A one-dimensional counterion distribution in the direction normal to the a–b plane, where polypeptoid and aqueous solution are taken to be continuous dielectric media with dielectric constants ε_p and ε_w, respectively. The boxes highlight the targeted ion and its image charge due to the dielectric mismatch.

dynamics (MD) simulations, we suggest that a possible molecular origin of such a peak shift is the image charge effect.

Modified Gaussian renormalized fluctuation theory. The atomic-scale cryo-EM images of Seidler *et al.*[19] show two rows of parallel crystalline peptoid molecules in V-shaped motifs, oriented in the a–c plane as shown in Figure 1(c). Our model assumes this morphology for the nanofiber. The protonated 4-aminophenyl groups lie in the a–b plane. These charged groups are introduced as fixed surface charges. Halogen counterions are distributed nearby to maintain charge neutrality of the system, in line with the experimental setup by Seidler *et al.*[19] This corresponds

to the "counterion-only" system in the EDL theory. The chemical system can be modeled by a rectangular cuboid with fixed charges on the a–b plane as shown in Figure 1(d). To further simplify the system, we ignore the edge effect and only consider a one-dimensional distribution of counterions in the direction perpendicular to the a–b plane as shown in Figure 1(e). This simplification is valid if the distance between the nanofiber surface and the counterion is small compared to the width of the nanofiber along the b axis (L_b = 16 Å).[27] Fixed $-NH_3^+$ groups are simplified as uniform surface charges, because the distance between fixed charges (a-spacing) L_a = 4.6 Å is less than the Bjerrum length of water, 7.1 Å. The surface charge density can thus be approximated by a uniform value $\sigma = 1\ e/L_aL_b = 1.36\ e/\mathrm{nm}^2$, where e is the elementary charge. The polypeptoid and aqueous solution are both taken to be continuous dielectric media with dielectric constants ε_p and ε_w, respectively, leading to a dielectric contrast at the interface.

To account for the dielectric mismatch at the polypeptoid interface, we apply the modified Gaussian renormalized fluctuation theory, which estimates the fluctuation of the electrostatic field using a Gaussian variational approach. The appearance of the self energy of ions in the Boltzmann factor unifies non-perturbative feedback of various effects including Born solvation energy, ion correlation, and long-range image force. The theory is particularly effective in modeling inhomogeneous electrolytes with spatially varying ion correlation and dielectric permittivity. It successfully captures anomalous phenomena driven by ion correlation, such as "charge inversion" and "like-charge attraction".[21,22,25,26] For a planar charged surface perpendicular to the z-axis, the theory yields the following self-consistent equations for the electrostatic potential $\psi(z)$, counterion

density $c_c(z)$, self energy of counterions $u_c(z)$, and correlation function $G(\mathbf{r}, \mathbf{r}')$:

$$-\nabla \cdot [\epsilon(z)\nabla\psi(z)] = \sigma\delta(z) + q_c c_c(z), \tag{1}$$

$$u_c(z) = \frac{q_c^2}{2} \int d\mathbf{r}' d\mathbf{r}'' h_c(\mathbf{r} - \mathbf{r}') G(\mathbf{r}', \mathbf{r}'') h_c(\mathbf{r} - \mathbf{r}''), \tag{2}$$

$$c_c(z) = \frac{n_c \exp\left[-q_c\psi(z) - u_c(z) - v_c\eta(z)\right]}{\int dz' \exp\left[-q_c\psi(z') - u_c(z') - v_c\eta(z')\right]}, \tag{3}$$

$$-\nabla_{\mathbf{r}'} \cdot \left[\epsilon(z')\nabla_{\mathbf{r}'} G(\mathbf{r}', \mathbf{r}'')\right] + 2I(z')G(\mathbf{r}', \mathbf{r}'') = \delta(\mathbf{r}' - \mathbf{r}''), \tag{4}$$

where $\epsilon(z) = k_B T \varepsilon_0 \varepsilon(z)/e^2$ is the scaled permittivity with ε_0 the vacuum permittivity, and $q_c = -1$ is the valence of counterions. Instead of using a point-charge model, we assume counterions have a finite charge spread in terms of a distribution function $h_c(\mathbf{r}, \mathbf{r}')$. For mathematical convenience, we consider $h_c(\mathbf{r}, \mathbf{r}')$ to be Gaussian. $n_c = \sigma/(|q_c|e)$ is the number of counterions per unit area determined by the surface charge density σ. $\eta(z) = -(1/v_w)\ln[1 - v_c c_c(z)]$ is the field that accounts for incompressibility with v_c and v_w, the excluded volume of counterions and solvent molecules, respectively. $2I(z) = \epsilon(z)\kappa^2(z) = q_c^2 c_c(z)$, where $I(z)$ and $\kappa(z)$ are the local ionic strength and the inverse of the screening length, respectively. The detailed derivation of the theory is provided in Section S1 of the Supporting Information.

The dielectric mismatch is modeled by a step function $\varepsilon(z) = \varepsilon_p$ for $z < 0$ and $\varepsilon(z) = \varepsilon_w$ for $z > 0$. This discontinuity of the dielectric constant leads to the boundary condition of the correlation function $G(\mathbf{r}', \mathbf{r}'')$ as a requirement of the continuity of the electric displacement in the normal direction, $\varepsilon_p \partial G(\mathbf{r}', \mathbf{r}'')/\partial z'|_{z'=0^-} = \varepsilon_w \partial G(\mathbf{r}', \mathbf{r}'')/\partial z'|_{z'=0^+}$. Due to the less polarizable nature of the polypeptoid, $\varepsilon_p = 7.5$ is used, a common value for the dielectric constant of less polarizable polymers such as polyethylene oxide (PEO).[28] In contrast, $\varepsilon_w = 80$ for the aqueous solution.

MD simulations. The simulation box consists of 24 polypeptoid chains and 24 Cl^- counterions solvated by 22000 water molecules. Similar to the experimental setup by Seidler *et al.*,[19] the simulations also consider the counterion-only system without the addition of extra salt ions. A CGenFF-based force field is adopted for the peptoid molecules,[29,30] and the TIP3P model is used

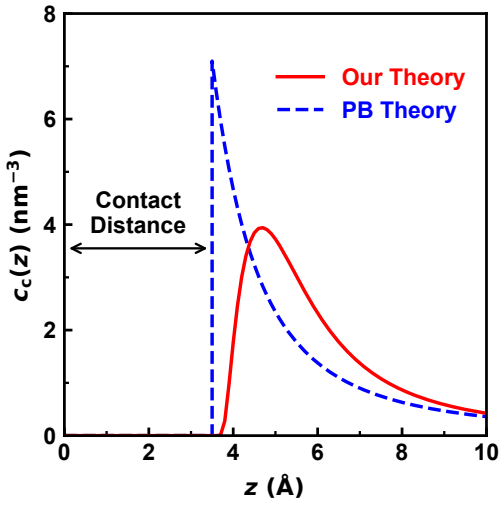


Figure 2: Density distribution $c_c(z)$ of counterions (Cl^-) as a function of distance z from the charged surface. The region within the closest contact distance $d = a_{-NH_3^+} + a_{Cl^-} = 3.50$ Å is inaccessible to counterions, where the radii of $-NH_3^+$ and Cl^- are 1.48 Å and 2.02 Å, respectively.[41,42] Surface charge density $\sigma = 1.36\ e/\text{nm}^2$ and dielectric constants $\varepsilon_p = 7.5$ (polypeptoids) and $\varepsilon_w = 80$ (water) are used here.

for water.[31] A cutoff distance of 12 Å is set for the van der Waals and electrostatic interactions. The particle-mesh Ewald summation is used for long-range electrostatic interactions.[32,33]

Simulations are performed using GROMACS 2022.3[34] in the NPT ensemble, following the previously reported protocol.[27,35–37] The system first undergoes 10 ns of Langevin dynamics at 450 K for structural relaxation, and is subsequently solvated and equilibrated in the NPT ensemble at 300 K and 1 atm. A Bussi thermostat is used to maintain the temperature,[38] and the Berendsen barostat followed by the Parrinello–Rahman barostat is used to maintain the pressure.[39,40] The equilibrium simulation is performed for 80 ns.

We first apply the modified Gaussian renormalized fluctuation theory to calculate the distribution of Cl^- near the charged polypeptoid surface, and the results are shown in Figure 2. We also plot the result obtained from classical PB theory for comparison. Due to the excluded volume of surface $-NH_3^+$ and counterions, the closest distance that the centers of counterions can access is $d = a_{-NH_3^+} + a_{Cl^-}$, where $a_{-NH_3^+}$ and a_{Cl^-} are the radii of $-NH_3^+$ and Cl^-, respectively. This leads to a region usually known as the Helmholtz layer. The PB theory predicts a monotonically decaying counterion distribution, with the peak exactly at $z = d$. The PB profile thus indicates

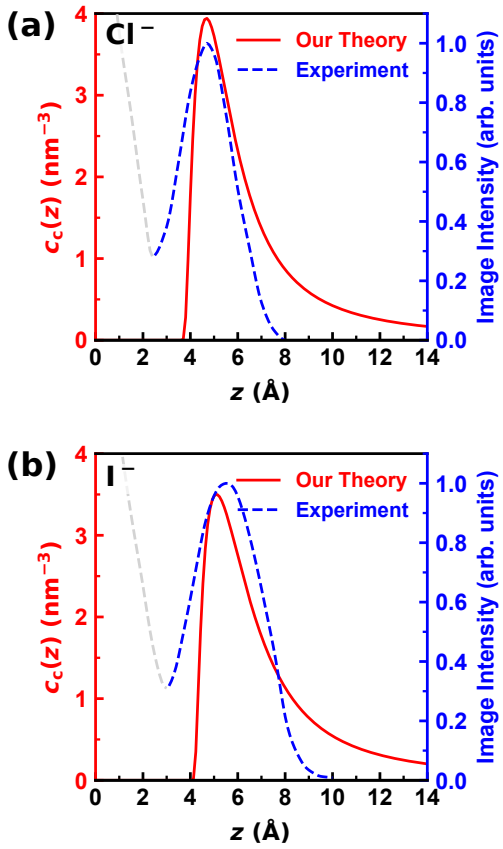


Figure 3: Comparison between our theoretical predictions and experimental results from cryo-EM images for counterion distributions of (a) Cl^- and (b) I^-. The radii of Cl^- and I^- are 2.02 Å and 2.45 Å, respectively.[41] Red lines show theoretical predictions of counterion density $c_c(z)$. Blue dashed lines show image intensities of counterions (normalized by the peak value) and gray dashed lines represent image intensities of polypeptoids. Experimental data are adapted from Seidler *et al.*[19]

that counterions are condensed directly at the outer Helmholtz plane, forming close contact with surface charges. In stark contrast, the counterion distribution predicted by our theory exhibits a non-monotonic shape, with the peak shifted by a distance of 1.2 Å from the outer Helmholtz plane. This shows a depletion of counterions from the polypeptoid surface, where the depletion region has to be occupied by solvent water molecules. The existence of a water layer between the surface charges and condensed counterions predicted by our theory is consistent with the observations from cryo-EM images by Seidler *et al.*[19] It should be noted that the calculated counterion distribution is not sensitive to the exact value of the dielectric constant of the polypeptoid as long as $\varepsilon_p \ll \varepsilon_w$ (see Section S2 in the Supporting Information).

To validate our theory, we perform a quantitative comparison between theoretical predictions

and experimental data from cryo-EM images. Figure 3 plots the theoretical counterion distributions together with the experimental image intensity profiles for two types of counterions. The radii of anions (a_{Cl^-} = 2.02 Å and a_{I^-} = 2.45 Å) are chosen to be their effective Born radii determined as the average of the crystal ionic radius and the first peak position in the ion-solvent radial distribution function,[41] whereas the radius of $-NH_3^+$ ($a_{-NH_3^+}$ = 1.48 Å) is the effective ionic radius determined from a bond-valence analysis.[42] For Cl^-, the peak position predicted by our theory is 4.70 Å, which matches the experimental results. For I^-, the theoretical peak position of 5.13 Å is also close to the experimental value 5.50 Å. The outward shift of the peak position of I^- compared to that of Cl^- is because the former has a larger contact distance due to its larger radius (i.e. $a_{I^-} > a_{Cl^-}$). Furthermore, the theoretical counterion distribution also has a shape similar to the image intensity for both types of counterions. The long tail in the theoretical counterion distribution represents the fraction of non-condensed counterions which diffuse in the aqueous solution and cannot be identified from cryo-EM images. Therefore, using literature-reported values of parameters, our theory shows quantitative agreement with experimental results of the counterion distribution.

A possible molecular origin of counterion depletion is the image charge repulsion caused by the dielectric mismatch at the polypeptoid–water interface. Because of the low dielectric constant of the polypeptoid nanofiber, the electrostatic field generated by a specific counterion in the vicinity of the interface gets distorted. This is equivalent to an effective image charge with the same sign appearing on the opposite side of the interface as illustrated in Figure 1(e). The image charge exerts a repulsive force on the targeted counterion itself, giving rise to the depletion region in the counterion distribution. Furthermore, the image charge repulsion originates from the fluctuation of the electrostatic field due to the appearance of a specific ion at a specific position near the interface, which is absent in the mean-field classical PB theory. By systematically incorporating this fluctuation effect as a long-range component of the self energy of ions, our theory successfully captures the image charge repulsion at the dielectric polypeptoid interface.

The peak position of the counterion distribution can be understood by a simple analysis of relevant length scales. Consider a test counterion of valence q_c at a distance z from the planar charged

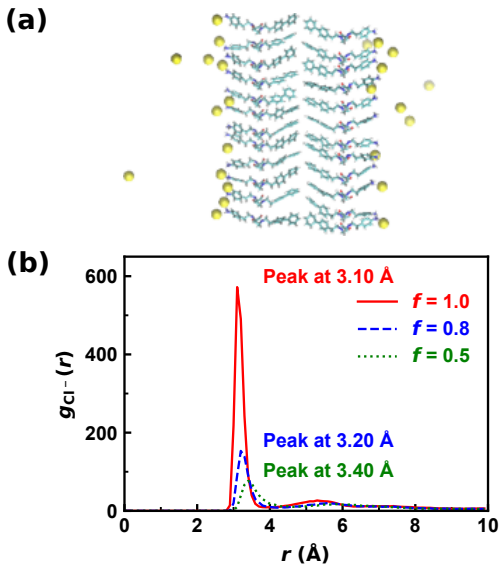


Figure 4: MD simulation of counterions condensed near the polypeptoid surface. (a) Snapshot of polypeptoid nanofiber and Cl^- (yellow spheres) in the simulations. (b) Radial distribution function $g_{Cl^-}(r)$ versus the distance r between $-NH_3^+$ and Cl^- in a pair for different rescaling factors of partial ionic charges $f = 1.0$, 0.8, and 0.5.

surface. This test ion bears the attraction from the charged surface as $E_{att} = 2\pi|q_c|l_B\sigma z = z/l_{GC}$. Meanwhile, the repulsion between the test ion and its own image charge is $E_{rep} = \gamma|q_c|^2 l_B/(2z)$. Here, $l_B = e^2/(4\pi\varepsilon_0\varepsilon_w k_B T)$ is the Bjerrum length of the solvent, and $l_{GC} = 1/(2\pi|q_c|\sigma l_B)$ is the Gouy–Chapman length. $\gamma = (\varepsilon_w - \varepsilon_p)/(\varepsilon_w + \varepsilon_p)$ represents the dielectric contrast between the solvent and polypeptoid. Balancing E_{att} and E_{rep} results in a characteristic distance $d_c = (\gamma/2)^{1/2}|q_c|(l_B l_{GC})^{1/2}$, which corresponds to the peak position in the counterion distribution. For $z < d_c$, image charge repulsion dominates, leading to a depletion layer of counterions in the vicinity of the charged surface. We note that there are discussions on the dielectric properties of water in the vicinity of different surfaces.[4,5] However, as long as $\varepsilon_w \gg \varepsilon_p$, we have $\gamma \approx 1$. The depletion layer is thus not sensitive to the exact value of the dielectric constant of water.

We also perform MD simulations to help understand the microscopic structure of counterion condensation. The snapshot in Figure 4(a) shows that condensed Cl^- and surface $-NH_3^+$ groups form contact ion pairs, without water molecules in the middle. This structural information can be more clearly presented by the radial distribution function $g_{Cl^-}(r)$, which reflects the probability of finding a Cl^- at a distance r from a $-NH_3^+$. As shown in Figure 4(b), $g_{Cl^-}(r)$ shows a sharp

first peak corresponding to close contact ion pairs and a rather small second peak corresponding to solvent-separated ion pairs. The first peak is much higher than the second peak, indicating the dominant fraction of close contact ion pairs. The position of the first peak is $r = 3.10$ Å, close to the sum of $a_{-NH_3^+}$ and a_{Cl^-} ($a_{-NH_3^+} = 1.48$ Å, $a_{Cl^-} = 2.02$ Å).[41,42] Similar results of close contact ion pairs and the absence of water molecules between them can also be obtained by plotting the density distributions of Cl^- and H_2O with respect to the charged surface (see Section S4 in the Supporting Information). The simulation results using non-polarizable force fields show the absence of water molecules between condensed counterions and surface charges.

Fixed atomic charges used in the current MD simulations do not capture charge polarization in response to the fluctuation of the electrostatic field. In the molecular description, the image charge effect represents the total equilibrium polarization response of the medium, which requires both the reorientation of the permanent dipole of molecules and the induced dipole due to electronic polarization. Although part of the molecular reorientation is already present in the MD simulations with fixed-charge force fields, electronic polarization is absent. An empirical approach to include the polarization effect is to reparameterize the force fields. In particular, the rescaling of partial ionic charges is usually employed in modeling electrochemical and biological systems to enforce an agreement between simulation and experiment.[43–45] Here, we also examine the effect of partial ionic charges on counterion condensation. Figure 4(b) shows that the peak position of $g_{Cl^-}(r)$ remains almost the same as we reduce the rescaling factor f of partial ionic charges from 1.0 to 0.5. Meanwhile, the peak value of $g_{Cl^-}(r)$ decreases for smaller f. The representative snapshots in MD simulations with $f = 0.8$ and 0.5 are provided in Section S3 of the Supporting Information. The rescaling approach thus does not alter the nature of counterion condensation in terms of close contact ion pairs but only changes the condensed fraction of counterions. Our work demonstrates that a simple rescaling of ionic charges cannot capture the electronic polarization at the molecular level and thus the corresponding dielectric response in the continuum description. A more systematic approach is to involve polarizable force fields based on quantum chemistry calculations to determine the atomic-level response to local dielectric and ionic environments.[46–49]

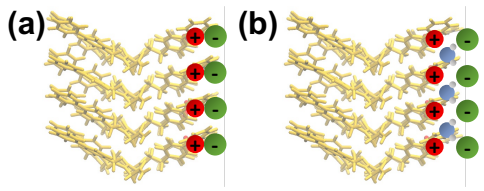


Figure 5: Schematic illustration of the microstructure of counterion condensation near a polypeptoid surface. (a) Close contact ion pairs predicted by classical PB theory and MD simulations with non-polarizable force fields and (b) the existence of water molecules between surface charges and condensed counterions to form solvent-separated ion pairs predicted by our theory.

The microstructure of counterion condensation predicted by our theory is qualitatively different from classical PB theory and MD simulations using non-polarizable force fields. As illustrated by Figure 5(a), both PB theory and MD simulations predict a close contact of condensed counterions and polypeptoid surface charges. In contrast, the peak position of the counterion distribution calculated by our theory exhibits a shift of 1.2 Å toward the aqueous solution, approximately the thickness of a water monolayer. As shown in Figure 5(b), our theory suggests the existence of a layer of water molecules between condensed counterions and polypeptoid surface charges, which thus well explains the puzzle observed in cryo-EM images by Seidler *et al.* [19]

In this work, we investigate the microscopic structure of counterion condensation near a charged polypeptoid surface by combining the modified Gaussian renormalized fluctuation theory and MD simulations. Our theory predicts a peak shift of condensed counterions by a distance approximately equal to the thickness of a water monolayer. Using only the intrinsic parameters of polypeptoid and ions, our theoretical predictions of both the peak position and the shape of the counterion distribution are in quantitative agreement with the results obtained from cryo-EM images. We provide a possible explanation for the formation of such solvent-separated ion pairs as the image charge repulsion near a dielectric interface. This important electrostatic feature cannot be captured by classical PB theory or MD simulations with non-polarizable force fields where electronic polarization is absent. Our work highlights the importance of the image charge effect arising from electrostatic fluctuations for the microstructure of electrical double layers. The modified Gaussian renormalized fluctuation theory systematically incorporates molecular information into the continuum description and can

be applied broadly to model the structural and dynamic behaviors of charged systems that existing theories fail to describe.

Acknowledgments

This work was supported by the U.S. Department of Energy, Office of Science, Basic Energy Sciences, Materials Sciences and Engineering Division under Contract No. DE-AC02-05-CH11231 within the Soft Matter Electron Microscopy Program (KC11BN). Computations were conducted on the Savio cluster at the University of California, Berkeley. We thank Dr. Yen Jea Lee for many helpful discussions.

References

(1) Israelachvili, J. N. *Intermolecular and Surface Forces*, 3rd ed.; Academic Press, 2011.

(2) Grosberg, A. Yu.; Nguyen, T. T.; Shklovskii, B. I. Colloquium : The Physics of Charge Inversion in Chemical and Biological Systems. *Rev. Mod. Phys.* **2002**, *74*, 329–345.

(3) Levin, Y. Electrostatic Correlations: From Plasma to Biology. *Rep. Prog. Phys.* **2002**, *65*, 1577–1632.

(4) Gonella, G.; Backus, E. H. G.; Nagata, Y.; Bonthuis, D. J.; Loche, P.; Schlaich, A.; Netz, R. R.; Kühnle, A.; McCrum, I. T.; Koper, M. T. M.; Wolf, M.; Winter, B.; Meijer, G.; Campen, R. K.; Bonn, M. Water at Charged Interfaces. *Nat. Rev. Chem.* **2021**, *5*, 466–485.

(5) Becker, M.; Loche, P.; Rezaei, M.; Wolde-Kidan, A.; Uematsu, Y.; Netz, R. R.; Bonthuis, D. J. Multiscale Modeling of Aqueous Electric Double Layers. *Chem. Rev.* **2024**, *124*, 1–26.

(6) Gouy, M. Sur la constitution de la charge électrique à la surface d'un électrolyte. *J. Phys. Theor. Appl.* **1910**, *9*, 457–468.

(7) Chapman, D. L. A contribution to the theory of electrocapillarity. *Philos. Mag.* **1913**, *25*, 475–481.

(8) Shin, S.-J.; Kim, D. H.; Bae, G.; Ringe, S.; Choi, H.; Lim, H.-K.; Choi, C. H.; Kim, H. On the Importance of the Electric Double Layer Structure in Aqueous Electrocatalysis. *Nat. Commun.* **2022**, *13*, 174.

(9) Griffin, J. M.; Forse, A. C.; Tsai, W.-Y.; Taberna, P.-L.; Simon, P.; Grey, C. P. In situ NMR and electrochemical quartz crystal microbalance techniques reveal the structure of the electrical double layer in supercapacitors. *Nat. Mater.* **2015**, *14*, 812–819.

(10) Forse, A. C.; Griffin, J. M.; Merlet, C.; Bayley, P. M.; Wang, H.; Simon, P.; Grey, C. P. NMR Study of Ion Dynamics and Charge Storage in Ionic Liquid Supercapacitors. *J. Am. Chem. Soc.* **2015**, *137*, 7231–7242.

(11) Zhou, Y.; Morais-Cabral, J. H.; Kaufman, A.; MacKinnon, R. Chemistry of Ion Coordination and Hydration Revealed by a K^+ Channel–Fab Complex at 2.0 Å Resolution. *Nature* **2001**, *414*, 43–48.

(12) Noskov, S. Y.; Bernèche, S.; Roux, B. Control of Ion Selectivity in Potassium Channels by Electrostatic and Dynamic Properties of Carbonyl Ligands. *Nature* **2004**, *431*, 830–834.

(13) Montes Ruiz-Cabello, F. J.; Trefalt, G.; Maroni, P.; Borkovec, M. Electric Double-Layer Potentials and Surface Regulation Properties Measured by Colloidal-Probe Atomic Force Microscopy. *Phys. Rev. E* **2014**, *90*, 012301.

(14) Siretanu, I.; Ebeling, D.; Andersson, M. P.; Stipp, S. L. S.; Philipse, A.; Stuart, M. C.; Van Den Ende, D.; Mugele, F. Direct Observation of Ionic Structure at Solid-Liquid Interfaces: A Deep Look into the Stern Layer. *Sci. Rep.* **2014**, *4*, 4956.

(15) Brown, M. A.; Abbas, Z.; Kleibert, A.; Green, R. G.; Goel, A.; May, S.; Squires, T. M.

Determination of Surface Potential and Electrical Double-Layer Structure at the Aqueous Electrolyte-Nanoparticle Interface. *Phys. Rev. X* **2016**, *6*, 011007.

(16) Favaro, M.; Jeong, B.; Ross, P. N.; Yano, J.; Hussain, Z.; Liu, Z.; Crumlin, E. J. Unravelling the Electrochemical Double Layer by Direct Probing of the Solid/Liquid Interface. *Nat. Commun.* **2016**, *7*, 12695.

(17) Griffin, L. R.; Browning, K. L.; Clarke, S. M.; Smith, A. M.; Perkin, S.; Skoda, M. W. A.; Norman, S. E. Direct Measurements of Ionic Liquid Layering at a Single Mica–Liquid Interface and in Nano-Films between Two Mica–Liquid Interfaces. *Phys. Chem. Chem. Phys.* **2017**, *19*, 297–304.

(18) Hurth, C.; Li, C.; Bard, A. J. Direct Probing of Electrical Double Layers by Scanning Electrochemical Potential Microscopy. *J. Phys. Chem. C* **2007**, *111*, 4620–4627.

(19) Seidler, M.; Yu, T.; Luo, X.; Prendergast, D.; Zuckermann, R. N.; Jiang, X.; Balsara, N. P. Atomic-Scale Imaging of Condensed Counterions. *Macromolecules* **2024**, *57*, 10016–10022.

(20) Wang, Z.-G. Fluctuation in Electrolyte Solutions: The Self Energy. *Phys. Rev. E* **2010**, *81*, 021501.

(21) Wang, R.; Wang, Z.-G. Effects of Image Charges on Double Layer Structure and Forces. *J. Chem. Phys.* **2013**, *139*, 124702.

(22) Wang, R.; Wang, Z.-G. On the Theoretical Description of Weakly Charged Surfaces. *J. Chem. Phys.* **2015**, *142*, 104705.

(23) Dos Santos, A. P.; Levin, Y. Ions at the Water–Oil Interface: Interfacial Tension of Electrolyte Solutions. *Langmuir* **2012**, *28*, 1304–1308.

(24) Jungwirth, P.; Tobias, D. J. Specific Ion Effects at the Air/Water Interface. *Chem. Rev.* **2006**, *106*, 1259–1281.

(25) Agrawal, N. R.; Wang, R. Electrostatic Correlation Induced Ion Condensation and Charge Inversion in Multivalent Electrolytes. *J. Chem. Theory Comput.* **2022**, *18*, 6271–6280.

(26) Agrawal, N. R.; Duan, C.; Wang, R. Nature of Overcharging and Charge Inversion in Electrical Double Layers. *J. Phys. Chem. B* **2024**, *128*, 303–311.

(27) Lee, Y. J.; Seidler, M.; Luo, X.; Butterfoss, G. L.; Yu, T.; Rad, B.; Xuan, S.; Zhu, C.; Prendergast, D.; Balsara, N. P.; Abel, B. A.; Zuckermann, R. N.; Jiang, X. Crystalline Peptoid Nanofibers with a Single-Unit Cell Cross Section. *J. Am. Chem. Soc.* **2025**, *147*, 27390–27402.

(28) Nakamura, I.; Balsara, N. P.; Wang, Z.-G. Thermodynamics of Ion-Containing Polymer Blends and Block Copolymers. *Phys. Rev. Lett.* **2011**, *107*, 198301.

(29) Vanommeslaeghe, K.; Hatcher, E.; Acharya, C.; Kundu, S.; Zhong, S.; Shim, J.; Darian, E.; Guvench, O.; Lopes, P.; Vorobyov, I.; Mackerell, A. D. CHARMM General Force Field: A Force Field for Drug-like Molecules Compatible with the CHARMM All-atom Additive Biological Force Fields. *J. Comput. Chem.* **2010**, *31*, 671–690.

(30) Weiser, L. J.; Santiso, E. E. A CGenFF-based Force Field for Simulations of Peptoids with Both Cis and Trans Peptide Bonds. *J. Comput. Chem.* **2019**, *40*, 1946–1956.

(31) Jorgensen, W. L.; Chandrasekhar, J.; Madura, J. D.; Impey, R. W.; Klein, M. L. Comparison of Simple Potential Functions for Simulating Liquid Water. *J. Chem. Phys.* **1983**, *79*, 926–935.

(32) Darden, T.; York, D.; Pedersen, L. Particle Mesh Ewald: An N·log(N) Method for Ewald Sums in Large Systems. *J. Chem. Phys.* **1993**, *98*, 10089–10092.

(33) Essmann, U.; Perera, L.; Berkowitz, M. L.; Darden, T.; Lee, H.; Pedersen, L. G. A Smooth Particle Mesh Ewald Method. *J. Chem. Phys.* **1995**, *103*, 8577–8593.

(34) Abraham, M. J.; Murtola, T.; Schulz, R.; Páll, S.; Smith, J. C.; Hess, B.; Lindahl, E. GROMACS: High Performance Molecular Simulations through Multi-Level Parallelism from Laptops to Supercomputers. *SoftwareX* **2015**, *1-2*, 19–25.

(35) Seidler, M.; Li, N. K.; Luo, X.; Xuan, S.; Zuckermann, R. N.; Balsara, N. P.; Prendergast, D.; Jiang, X. Importance of the Positively Charged σ-Hole in Crystal Engineering of Halogenated Polypeptoids. *J. Phys. Chem. B* **2022**, *126*, 4152–4159.

(36) Yu, T.; Luo, X.; Prendergast, D.; Butterfoss, G. L.; Rad, B.; Balsara, N. P.; Zuckermann, R. N.; Jiang, X. Structural Elucidation of a Polypeptoid Chain in a Crystalline Lattice Reveals Key Morphology-Directing Role of the N-Terminus. *ACS Nano* **2023**, *17*, 4958–4970.

(37) Luo, X.; Yu, T.; Li, N. K.; Zuckermann, R. N.; Jiang, X.; Balsara, N. P.; Prendergast, D. Thermodynamic Driving Forces for the Self-Assembly of Diblock Polypeptoids. *ACS Nano* **2024**, *18*, 14917–14924.

(38) Bussi, G.; Donadio, D.; Parrinello, M. Canonical Sampling through Velocity Rescaling. *J. Chem. Phys.* **2007**, *126*, 014101.

(39) Parrinello, M.; Rahman, A. Polymorphic Transitions in Single Crystals: A New Molecular Dynamics Method. *J. Appl. Phys.* **1981**, *52*, 7182–7190.

(40) Berendsen, H. J. C.; Postma, J. P. M.; van Gunsteren, W. F.; DiNola, A.; Haak, J. R. Molecular Dynamics with Coupling to an External Bath. *J. Chem. Phys.* **1984**, *81*, 3684–3690.

(41) Satheesan Babu, C.; Lim, C. A New Interpretation of the Effective Born Radius from Simulation and Experiment. *Chem. Phys. Lett.* **1999**, *310*, 225–228.

(42) Sidey, V. On the Effective Ionic Radii for Ammonium. *Acta Crystallogr., Sect. B: Struct. Sci., Cryst. Eng. Mater.* **2016**, *72*, 626–633.

(43) Leontyev, I.; Stuchebrukhov, A. Accounting for Electronic Polarization in Non-Polarizable Force Fields. *Phys. Chem. Chem. Phys.* **2011**, *13*, 2613–2626.

(44) Kirby, B. J.; Jungwirth, P. Charge Scaling Manifesto: A Way of Reconciling the Inherently Macroscopic and Microscopic Natures of Molecular Simulations. *J. Phys. Chem. Lett.* **2019**, *10*, 7531–7536.

(45) Duboué-Dijon, E.; Javanainen, M.; Delcroix, P.; Jungwirth, P.; Martinez-Seara, H. A Practical Guide to Biologically Relevant Molecular Simulations with Charge Scaling for Electronic Polarization. *J. Chem. Phys.* **2020**, *153*, 050901.

(46) Ponder, J. W.; Wu, C.; Ren, P.; Pande, V. S.; Chodera, J. D.; Schnieders, M. J.; Haque, I.; Mobley, D. L.; Lambrecht, D. S.; DiStasio, R. A.; Head-Gordon, M.; Clark, G. N. I.; Johnson, M. E.; Head-Gordon, T. Current Status of the AMOEBA Polarizable Force Field. *J. Phys. Chem. B* **2010**, *114*, 2549–2564.

(47) Huang, L.; Roux, B. Automated Force Field Parameterization for Nonpolarizable and Polarizable Atomic Models Based on Ab Initio Target Data. *J. Chem. Theory Comput.* **2013**, *9*, 3543–3556.

(48) Lemkul, J. A.; Huang, J.; Roux, B.; MacKerell, A. D. An Empirical Polarizable Force Field Based on the Classical Drude Oscillator Model: Development History and Recent Applications. *Chem. Rev.* **2016**, *116*, 4983–5013.

(49) Lin, F.-Y.; MacKerell, A. D. Improved Modeling of Cation-π and Anion-Ring Interactions Using the Drude Polarizable Empirical Force Field for Proteins. *J. Comput. Chem.* **2020**, *41*, 439–448.

Table of Contents Graphic

For Table of Contents Use Only

Understanding the Microscopic Structure of Counterion Condensation Near a Charged Polypeptoid Surface

Xiaohui Zhang, Luofu Liu, Xi Jiang, Ronald N. Zuckermann, David Prendergast, Nitash P. Balsara, and Rui Wang

